IEEE Access
Multidisciplinary | Rapid Review | Open Access Journal

Received February 16, 2021, accepted April 13, 2021, date of publication April 20, 2021, date of current version April 27, 2021.

Digital Object Identifier 10.1109/ACCESS.2021.3074317

Conformal Antenna Array Design Using Aperture Synthesis and On-Platform Modeling

TIMOTHY G. PELHAM[1], (Member, IEEE), GEOFF HILTON[1], EVANGELOS MELLIOS[1], AND ROB LEWIS[2], (Member, IEEE)

[1]Department of Electrical and Electronic Engineering, University of Bristol, Bristol BS8 1TR, U.K.
[2]BAE Systems Applied Intelligence Laboratories, Great Baddow CM2 8HN, U.K.

Corresponding author: Timothy G. Pelham (t.g.pelham@bristol.ac.uk)

This work was supported in part by the BAE Systems Applied Intelligence Laboratories, Great Baddow, U.K., and in part by the EPSRC Centre for Doctoral Training in Communications under Grant EP/I028153/1.

ABSTRACT Conformal antenna arrays have long represented an attractive solution to challenges imposed by an electromagnetic aperture on an aerospace platform. This allows designers to trade between array positioning and geometry, and avoids the significant aerodynamic drag of a planar array. This is hampered by the expense of the design and computational modelling required to ensure that a conformal array will meet its performance requirements. The proposed approach uses raycasting techniques to predict the rectilinear projection of a conformal aperture onto the farfield to calculate the maximum achievable beam coverage (aperture maximum directivity envelope). In order to compare aperture projection with the performance of the modelled arrays in a consistent manner, the steering efficiency (SE), which is the fraction of the farfield steerable to within 3dB of the maximum directivity, was calculated for the aperture, stacked patch, and conical monopole elements. The stacked patch elements demonstrated a SE of 18% over the steering plane compared with 40% for the arbitrary directional elements, and the optimum of 38% for the aperture overall. The Conical monopole elements achieved a SE of 8%, compared to 20% for the measured elements, and 33% achieved with arbitrary omnidirectional elements. These results demonstrate that, for both omnidirectional and directional elements, the aperture projection method offers a compelling tool for conformal array design, which is consistent with the achieved array performance for the stacked patch and conical monopole elements.

INDEX TERMS Antenna array design, aperture synthesis, conformal antenna array, steering efficiency.

I. INTRODUCTION

Conformal antenna arrays can be viewed as the general case for antenna array design, with planar arrays representing a particular subset of the overall design space [1]. Any successful design strategy for conformal antenna arrays must reduce both the overall cost of design and the initial technical risk involved that could reasonably be expected to require multiple development cycles to reach the system performance goals, at least with current design methods [2].

There are two major approaches to the problem of predicting the performance of conformal antenna arrays; analytic and numerical. The analytic approach uses a series of connected equations to derive the expected farfield array directivity for the surface of interest, either based on a series of small planar arrays integrated into a curve [3], or based upon the projected area of the described curve [1]. The benefit of these methods is that it lends itself to some form of optimizing function to support overall array design based upon a suitable performance metric such as the power-aperture gain product (PAG) [4], [5]. The drawback, however, is that these methods are limited to those surfaces for which an analytic description is convenient, such as cylindrical, spherical and parabolic curves, or arrangements of planar faces.

The numerical approaches include full Electromagnetic (EM) models such as CST and HFSS [6], [7], based upon a detailed antenna array design and full wave simulations of the performance of each antenna element within the array. The drawback to this method is that the it necessitates the design process for the array in advance of a reliable prediction of the performance of the antenna array. In order to try and work around these limitations, there has been continuing

The associate editor coordinating the review of this manuscript and approving it for publication was Yasar Amin.

research in the aerospace field on different design strategies for antenna arrays for conformal surfaces, but still isolated from the platform, due to concerns around the excessive computational burden this would impose [8], [9].

In order to enable a systematic design process, a high level design tool is required that allows the design team to make assessments of the influence of electrically large platforms on the farfield beam coverage, without the initial investment of large computing clusters and design effort. If such a design tool were implemented, it could dramatically reduce the development costs for an integrated conformal array on electrically large platforms, while also supporting development of planar arrays. The closest approach to that presented here is the use of uniform theory of diffraction (UTD) based rays to predict the array radiation pattern of a conformal aperture on a locally convex conducting surface [10]. The strength of the UTD approach is its efficiency for larger arrays compared to conventional electro-magnetic models. However, it does not consider the effects of the aperture platform on the farfield performance, which may well be significant. This may take the form of large 'shadows' in the farfield pattern produced by the platform itself, which can only be considered correctly in the context of a model that considers the whole platform geometry.

The approach being proposed here is based upon the use of ray-casting techniques to generate a 'shadow map' of the rectilinear projection of the aperture on the platform of interest. The primary benefit is that the computational overhead is directly linked to the electrical size of the aperture itself, rather than that of the host platform [11]. The constrained information set allows this technique to be applied as an evaluation tool to assess the performance implications of antenna array size, shape and location on the farfield beamformed performance at an early stage in the design process, allowing conclusions to be drawn on the performance-cost relationship for different array design choices with minimal investment. This method concentrates on the farfield performance implications of aperture geometry and its location on a given platform. This is accomplished by predicting a realistic 'upper bound' on array performance for a given geometry, 'de-risking' a set of space and siting constraints before development using conventional EM solvers, while also providing a metric to assess the fitness of the resultant array design.

This method defines the 'optimum' performance of an aperture geometry in a specific direction to be the beamformed farfield directivity that meets the maximum directivity envelope of the aperture. This is calculated using the standard definition of directivity for the rectilinear projected area of the aperture over the full 3D space [12].

In this paper, the work flow required for conformal antenna array design on a complex platform is examined. The process starts with a notional aperture on a complex platform to establish the maximum directivity envelope for the planned array. A limited sub-array is introduced for clarity, and the effectiveness of different arbitrary element types upon the achievable antenna array performance is explored. The accuracy of this method is then assessed by designing and modelling a patch antenna and a monopole antenna element. A number of different beam forming and antenna array performance metrics are then used to compare aperture projection & arbitrary element methods against CST modelled and measured patterns.

II. PLATFORM ANALYSIS & APERTURE PROJECTION

A. APERTURE PROJECTION

In order to calculate an accurate projection for the proposed aperture, the plane of projection must be defined. When dealing with spherical coordinates this can be done conveniently by specifying the projection plane normal vector $\hat{n}$ in terms of (θ, ϕ). Thus, for aperture A with outward pointing normal vector $\hat{k}$, within surface S the projected area A_p in direction $\hat{n}$ is found from Equation 1. This is shown in Figure 1 for an 8 element sub-array. This can be conveniently be rephrased in terms of a spherical farfield at distance R from the origin, and θ, ϕ coordinates.

$$A_p = \iint_S \vec{A} \,.\, \vec{\hat{n}}\, dS = \iint_R \vec{A} \,.\hat{n} \frac{d\theta d\phi}{|\,\vec{n} \,.\, \vec{k}\,|} \tag{1}$$

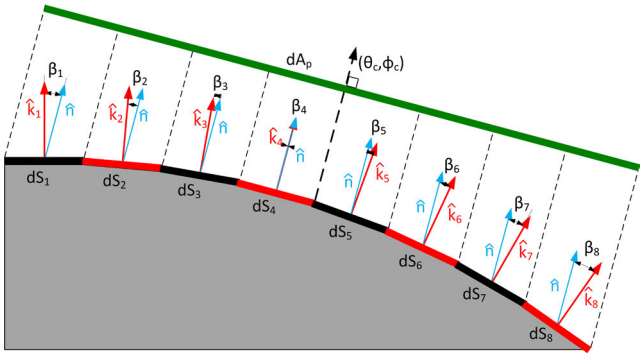

FIGURE 1. Projected area dA_p in the context of 8 element array with surfaces $dS_{1..8}$ and associated normals $\hat{k_m}$ and farfield pointing vector $\hat{n}$ associated with command angle vector (θ_c, ϕ_c).

Naturally this depends upon a surface geometry defined via a convenient function. However in the limit of an infinitesimally small area of A, dA_p can be defined in terms of dS and β_m, which is the angle between $\hat{n}$ and $\hat{k}$, as shown in Equation 2. This limit can then be used in terms of a Riemann sum by dividing the aperture into M facets, each with its own area A_m and normal vector $\hat{k}_m$ for $m = [1, \ldots, M]$. These aperture facets are defined in terms of their corner vertices, centroid coordinates, and outward pointing normal vector.

$$dA_p = \cos\beta_m dS \tag{2}$$

When combined with the raycaster mapping, a sub-set M_{RC} is found as the visible facets for the farfield coordinates defined by the projection plane normal vector $\hat{n}$, and this is used to define A_p in Equation 3 as the visible projected area from aperture A in direction $\hat{n}$.

$$A_p = \sum_{m=M_{RC}} A_m \cos\beta_m \tag{3}$$

This can then be used to calculate the maximum directivity of the aperture in that direction [13], and for a wavelength of interest λ, shown in Equation 4.

$$D_{max}(\hat{n}) = \frac{4\pi A_p}{\lambda^2} \tag{4}$$

This process can then be repeated for each farfield point of interest, until a full 3D prediction of the *aperture maximum directivity envelope* has been generated via Equations 3 & 4. This metric, based upon the defined aperture, represents the maximum achievable directivity for the beamformed array over the 3D space.

B. PLATFORM ANALYSIS

There are many platforms of interest for conformal antenna array design. If aperture surfaces are categorised in terms of radius of curvature and directions of curve, then aerospace platforms could easily be considered the most challenging class. The combination of extremely limited surface area and sharply curved surfaces present a challenge to any conventional antenna array design approach. These platforms could include smaller unmanned aerial vehicles (UAVs) such as the ScanEagle, larger Unmanned Combat Air Vehicle (UCAV) such as the X-47B, manned strike aircraft, or larger aircraft such as the E-8, or their successors [14]–[16]. However, while there are a large number of platforms of interest, any responsible publication into the design of conformal antenna arrays integrated into an aerospace platform cannot be based on any airframe currently deployed. Therefore a suitable host platform was required to allow the design process to be considered, with features similar to modern aircraft.

The de Havilland Sea Vixen was selected, based principally upon its relatively high drag 'thick' wings [17]. This aerofoil profile is not common in modern supersonic fighter aircraft. However, with the continuing development of UCAV as a concept, this kind of wing profile is becoming increasingly relevant once again. The fuselage and wing 'booms' also offer a substantial variety of curved surfaces that can be conveniently considered as possible locations for conformal antenna arrays. In this example, the lower portion of the starboard boom will be considered as the proposed site for a conformal antenna array, suitable for electronic warfare or wideband communications systems. The proposed complete aperture shown at the centre of the aperture maximum directivity envelope (Figure 2) has a total aperture surface area of $0.118m^2$. A planar array of this size would be expected to produce a maximum directivity of around 28dBi at 6GHz.

In order to predict the maximum directivity envelope for this aperture, a 3D model of the de Havilland Sea Vixen was created based upon the published technical drawings and aerofoil in the Stereo Lithography format (STL). This model was used, together with conformal aperture projection, to predict both the maximum aperture directivity for the desired farfield points [18] and also the effect of the platform on the maximum directivity envelope.

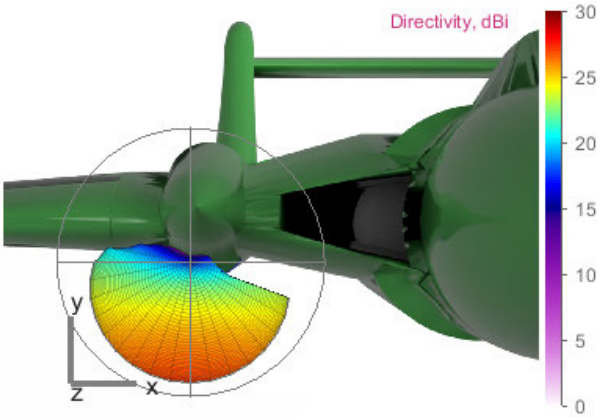

FIGURE 2. Modelled aperture on platform starboard boom, with maximum aperture directivity envelope (6GHz).

The resultant farfield pattern for the selected cylindrically curved array, sited on the lower starboard boom of the Sea Vixen, is shown in Figure 2 with the calculated aperture maximum directivity envelope. This pattern is shown in 2D format in Figure 3 in terms of command angles (θ_c, ϕ_c). The command angles (θ_c, ϕ_c), are defined in platform centric coordinates, $\theta_c = 0°$ along the direction of flight, with the aircraft horizon aligned along the x axis. From this, the aperture location at the base of the starboard boom cone can be deduced from the even coverage in the $\theta_c = 0° - 20°, \phi_c = 0° - 360°$ region. The large void imposed by the airframe clearly visible in the range $\theta_c = 30° - 180°$, $\phi_c = 0° - 180°$.

There are two caveats to this method. The first is that the maximum directivity is related to the effective area of the aperture rather than the physical area, and the exact correlation is not well defined. If produced by fringing effects the error should decrease as the overall aperture size increases and the proportional effects are reduced. The second is that this method is a geometric projection that does not account for the antenna element patterns or polarization employed in a given array.

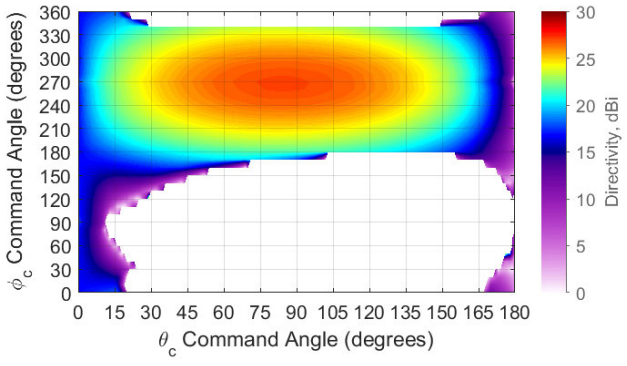

FIGURE 3. Maximum aperture directivity envelope (6GHz), in platform θ, ϕ axes.

C. APERTURE SYNTHESIS

In order to investigate this relationship between the aperture maximum directivity envelope, the antenna element pattern, and the achieved beamformed directivity, a limited array was defined. Using the surface geometry of the envisaged boom aperture within the airframe, an 8 element linear array was selected as an appropriate sub-array of the initial aperture. The conformal surface in this region is singly curved, and cylindrical, with a radius of curvature of 0.3m, or 6λ at 6GHz, and a total surface area of $0.005m^2$.

The aperture model prediction for this linear sub-array (Figure 4) is shown in Figure 5. This prediction can be intuitively understood by considering the projection of the surface area of the modelled 3D array elements onto the farfield. If the aperture model was a flat section along the curve, the maxima would be expected in the $\phi_c = 270°$ plane, however the 3D model was selected to account for elements with a 3D structure forward of the ground plane. Thus the ϕ_c maxima at 200° & 340° can be understood as the sum of the projected top and each side, respectively. The coverage within the region $\phi_c = 180° - 360°$ is extended due to the direction of curvature of the conformal surface, along the $\phi = 270°$ axis. The maxima in the region between $\theta_c = 30°$ and $\theta_c = 45°$ is a consequence of the array normal vectors oriented along $\phi = 270°$ in the range $\theta = [0° : 5° : 35°]$ with a mean normal of $\theta = 17.5°$. The maxima represents the region of maximum convergence between the projected area of each element, as can be seen from Figure 1 & 4.

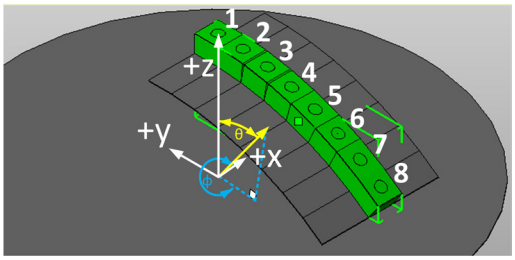

FIGURE 4. Aperture model of the 8-element sub array, with the aperture highlighted in green.

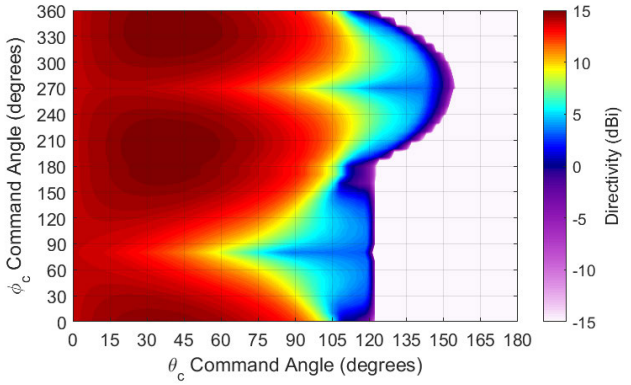

FIGURE 5. Maximum directivity envelope (6GHz) for 8 element array with shielding plate.

This form of directivity envelope prediction gives an excellent understanding of the potential performance of an aperture, however it does not consider the behaviour of different types of antenna element patterns. In order to address this, a set of arbitrary element patterns were devised to investigate the effects of different antenna element patterns within the confines of the chosen conformal surface. This approach defined a set of isotropic, directional, and omnidirectional sources with coordinates and outward pointing normal vectors consistent with the 8 element linear conformal array and the appropriate truncation boundary for each element farfield pattern. This provides a basic model for the effects of a ground plane for each element, radiating into half space.

The orientation of each element's half space is defined by the element's outward pointing normal vector.

The isotropic element patterns were defined as a unitary magnitude farfield pattern, truncated to the visible half space, defined by each element's normal vector. The total directivity patterns for the truncated isotropic elements are shown in Figure 6 for element 1, and the Y-Z plane for elements [1, 4, 8] in Figure 7. The element patterns, beamformed to direct the maximum to $(\theta_c, \phi_c) = (45°, 270°)$ is shown in Figure 8 in total directivity form.

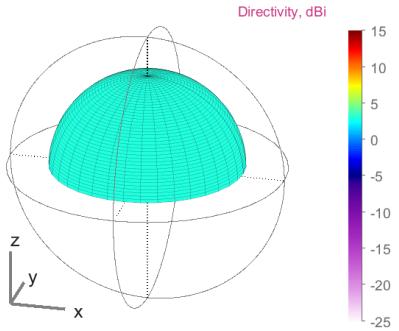

FIGURE 6. Cropped isotropic element total directivity pattern for element 1.

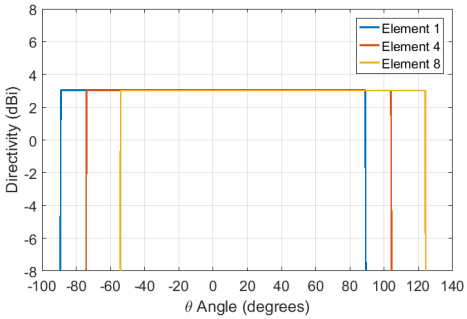

FIGURE 7. Cropped isotropic elements total directivity patterns on the Y-Z plane.

The omnidirectional pattern was fixed as a normalised sinc function rotationally symmetric around the element normal vector. A maxima was fixed, 65° offset from the normal vector and the whole farfield truncated to the element's visible

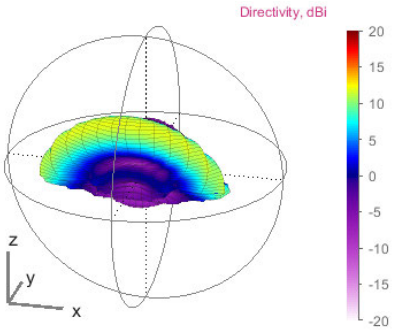

FIGURE 8. Cropped isotropic beamformed array pattern, steered towards $(\theta_c, \phi_c) = (45°, 270°)$.

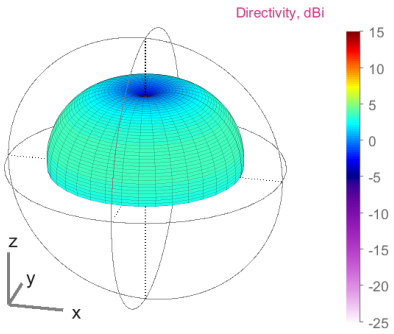

FIGURE 9. Cropped omnidirectional element total directivity pattern for element 1.

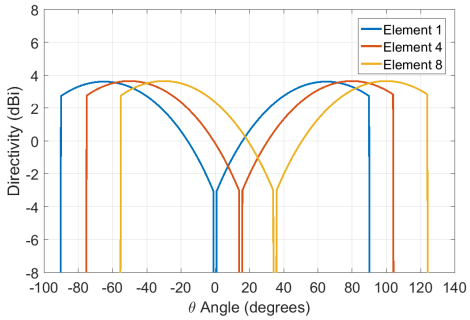

FIGURE 10. Cropped omnidirectional elements total directivity patterns on the Y-Z plane.

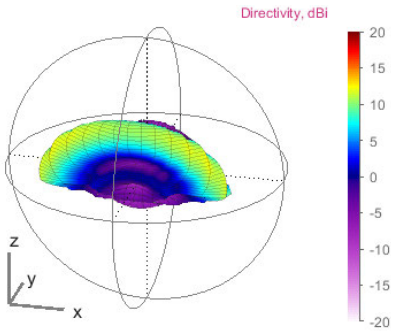

FIGURE 11. Cropped omnidirectional beamformed array pattern, steered towards $(\theta_c, \phi_c) = (45°, 270°)$.

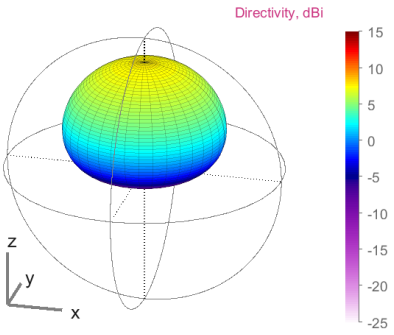

FIGURE 12. Cropped directional element total directivity pattern for element 1.

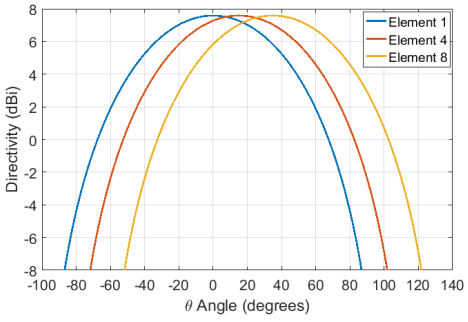

FIGURE 13. Cropped directional elements total directivity patterns on the Y-Z plane.

half space. The total directivity patterns for the truncated isotropic elements are shown in Figure 9 for element 1, and the Y-Z plane for elements $[1, 4, 8]$ in Figure 10. The total beamformed array pattern, steered towards $(\theta_c, \phi_c) = (45°, 270°)$, is shown in Figure 11.

The directional element's farfield pattern was defined using a normalised sinc function with a unitary linear maxima aligned along the element normal vector, and a half power beamwidth of 90°, and the whole farfield truncated to the element's visible half space. The total directivity patterns for the truncated isotropic elements are shown in Figure 12 for element 1, and the Y-Z plane for elements $[1, 4, 8]$ in Figure 13. The total beamformed array pattern, steered towards $(\theta_c, \phi_c) = (45°, 270°)$, is shown in Figure 14.

In order to ensure that a viable comparison can be drawn between the predicted maximum directivity envelope and the beamformed achieved directivity for each array, an optimising beamforming method is required. While finding the true 'optimum' beamforming weights for a given command angle set and performance criterion (maximum gain, maximum sidelobe level) is not always possible, a combination approach can be used to search for the optimum. This approach performs four separate beamforming algorithms (Coherent Wavefront, Equal Gain Combining [19], Least Mean Squares [20]–[22] and Successive Projection [23]) for each set of command angles, and then the maximum achieved gain is selected. A true optimum set of weights is not guaranteed by these methods unless the antenna patterns are convex,

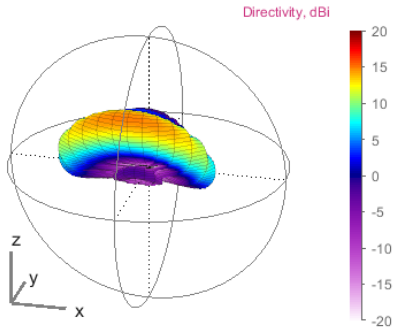

FIGURE 14. Cropped directional beamformed array pattern, steered towards $(\theta_c, \phi_c) = (45°, 270°)$.

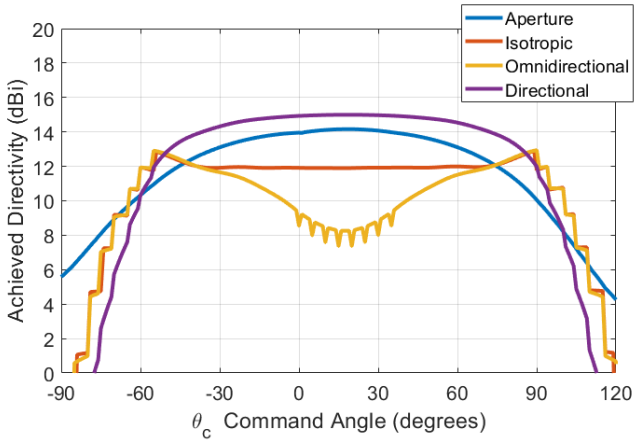

FIGURE 15. Comparison of Aperture projection, truncated Isotropic, Directional and Omnidirectional elements.

but this represents a reasonable compromise for this work. In order to minimise the null steering associated with steering along the Y-Z plane, along the normal aligned nulls of each antenna element, cylindrical coordinate mapping was used for the beamforming.

The array beam was then steered using cylindrical mapping (aligned with the x axis) and the polar angle ($\theta = 0°$ aligned with the positive Z axis). The comparison of the achieved directivity for each arbitrary element type steered to polar angles $\theta_c = 0° - 180°$ is shown in Figure 15. This gives the response that is expected intuitively. The directional element pattern, when compared to the aperture prediction, shows good agreement ($\leq 1.5dB$) in the region $\theta_c = 0° - 60°$ with a maxima at $\theta_c = 17.5°$, which is as expected based on the mean of element normal vectors. The omnidirectional element displays an overall null along these normal vectors, which is consistent with the expectation for an omnidirectional element. The 8 notches in Figure 15 indicate the angular alignment of each elements normal vector, and hence null vector, showing the overall array null position as the average of 8 individual nulls.

III. ARRAY MODELLING

A. ARRAY DESIGN

If the aperture directivity envelope, shown in Figure 5 and the achieved directivity of the arbitrary elements in Figure 15

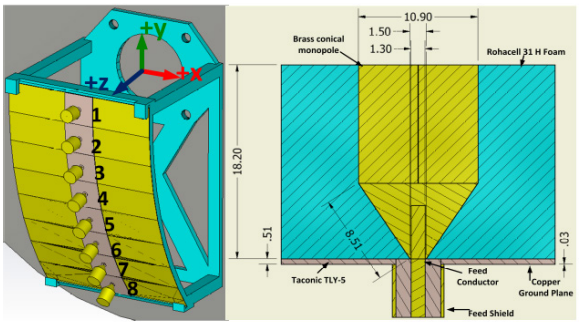

FIGURE 16. Conical monopole antenna elements.

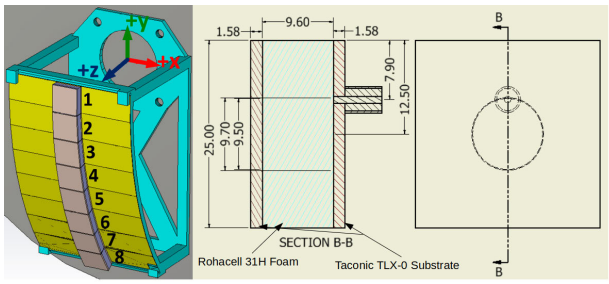

FIGURE 17. Stacked patch antenna elements.

are considered in concert, they give an understanding of the performance implications on the platform. A directive element can be expected to meet the maximum directivity criterion in the region $\theta_c = 0° - 60°$. The omnidirectional element would be expected to meet the criterion in the region $\theta_c = 60° - 105°$ for an individual element farfield maxima of 60° from the element normal, as shown in Figure 10.

A conical monopole Figure 16, was chosen as the omnidirectional element [24]. This had a -10dB impedance bandwidth of 3GHz-12GHz. A dual circular patch arrangement was chosen for the directive element, which had a -10dB impedance bandwidth of 5.29GHz-6.3GHz. The stacked patch design allowed an increased bandwidth and directivity in a very similar volume and had an identical inter-element pitch of 25mm (0.5λ at 6GHz) as with the conical monopole [25], Figure 17. Both antenna arrays were designed and simulated using CST Microwave Studio [6], exporting each embedded antenna pattern independently for beamforming.

As both the stacked patch and the conical monopole are strongly linearly polarized, the total directivity patterns are shown for clarity. This also enables clearer comparisons to the arbitrary elements to be drawn. The total directivity patterns for the stacked patch element 1 are shown in Figure 18 for element 1, and the y-z plane for all elements in Figure 21. The total directivity patterns for the conical monopole element 1 are shown in Figure 20 for element 1, and the y-z plane for all elements in Figure 22.

B. RESULTS

Using the arbitrary element patterns and maximum directivity envelope predictions as references, a comparison between the performance of each element type can be drawn. If the

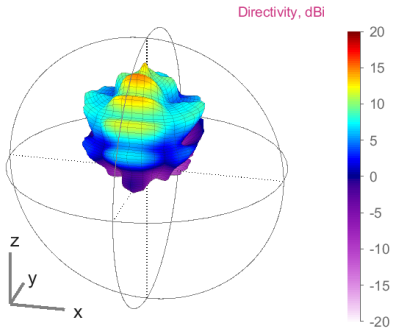

FIGURE 18. Patch element total directivity pattern for element 1.

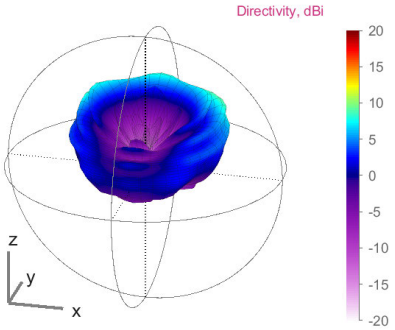

FIGURE 19. Conical monopole element total directivity pattern for element 1.

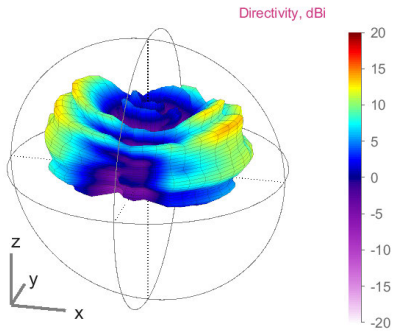

FIGURE 20. Conical monopole measured element total directivity pattern for element 1.

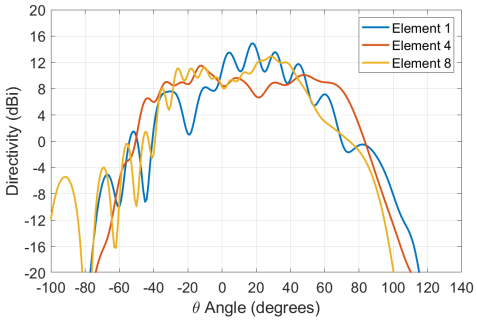

FIGURE 21. Patch elements total directivity patterns on the Y-Z plane.

stacked patch element 1's 3D farfield total directivity pattern in Figure 18 and the 2D total directivity slices in Figure 21 are compared to the directional arbitrary element patterns

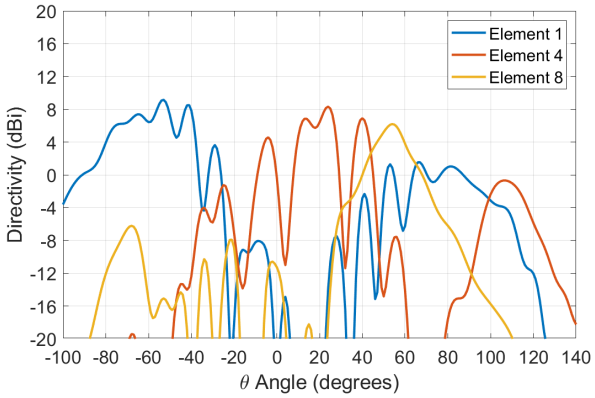

FIGURE 22. Conical monopole elements total directivity patterns on the Y-Z plane.

in Figures 12 & 13, it can be seen that the maxima of the stacked patch element is at least 4dB higher than that of the arbitrary directional element. This highlights a challenge to the use of arbitrary defined farfield patterns. In order to accurately predict the behaviour of an array of elements, some standard definition is required, such as using the element 'pitch' to normalise the maximum directivity of the arbitrary element.

If the conical monopole element 1's 3D farfield total directivity pattern in Figure 20 and the 2D total directivity slices in Figure 22 are compared to the omnidirectional arbitrary element patterns in Figures 9 & 10, it can be seen that the element has a higher maximum directivity and wider nulls than the arbitrary patterns.

The reasons for this can be observed by considering Figure 10, which compares the 2D total directivity element patterns for the arbitrary omnidirectional element and the equivalent comparison for the actual conical monopole element in Figure 22. In both cases the nulls of these elements are aligned along the Y-Z plane, and hence while beamforming in this plane is desirable for comparisons between the directional and omnidirectional elements, the effects of the element nulls are enhanced in comparison.

This comparison illustrates the agreement between the arbitrary omnidirectional element, and the conical pattern in general trends like null centre positions and maxima position. However, the maximum directivity of the modelled conical patterns is more than 4dB higher than the omnidirectional arbitrary elements.

When the other conical monopole element patterns are considered, instead of the wider null in the region $\theta = 0° - 60°$ as predicted by the arbitrary omnidirectional patterns, there are two null regions ($\theta_c = 0° - 20°$ & $\theta_c = 60° - 90°$) due to clustering maxima in the regions of $\theta_c = 30°$ and $\theta_c = 105°$ for elements 2-7.

When the measured conical monopole element patterns are examined, there is closer agreement between the maximum measured directivity of the elements and the arbitrary omnidirectional element patterns in the Y-Z plane, as shown

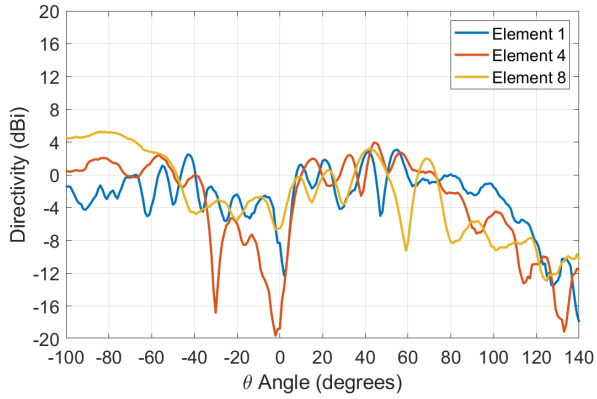

FIGURE 23. Conical monopole measured elements total directivity patterns on the Y-Z plane.

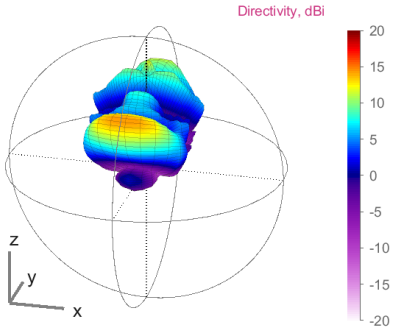

FIGURE 24. Patch beamformed array pattern, steered towards $(\theta_c, \phi_c) = (45°, 270°)$.

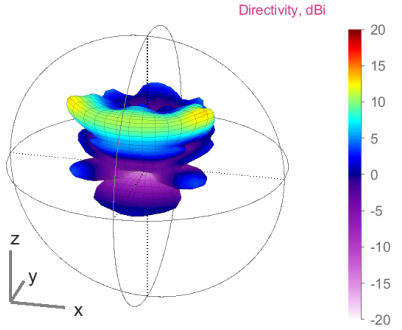

FIGURE 25. Conical monopole element beamformed array pattern, steered towards $(\theta_c, \phi_c) = (45°, 270°)$.

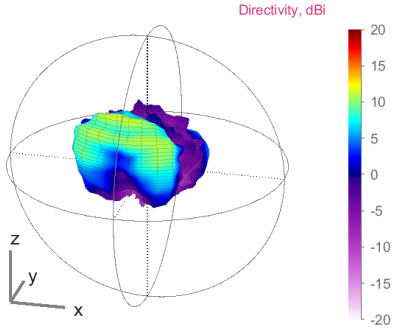

FIGURE 26. Measured Conical monopole element beamformed array pattern, steered towards $(\theta_c, \phi_c) = (45°, 270°)$.

in Figure 23. However, comparison of the modelled and measured element 1 patterns in Figures 19 and 20 shows that this is due to the measured element, radiating strongly along the x axis out of the analysis plane, while the modelled pattern peak directivity is within the plane ($\theta = -53°$).

What is most useful about this type of element analysis is that both the omnidirectional and the patch elements show general agreement with the predictions of the aperture prediction method. There is, however, some magnitude error due to differences in the effective aperture from that defined for aperture projection. At some angles the patch element is up to 5.4dB more directive than the predicted maximum. This indicates that the conformal ground plane is increasing the effective area of the array at this frequency (aperture boundary uncertainty), and this type of error can be expected to be minimised with larger, nonlinear arrays as the aperture boundary uncertainty would be a smaller fraction of the expected aperture. Poynting streamline analysis has been suggested as a useful method for calculating the effective area of an antenna or array [26]. This does, however, require an existing antenna or antenna array design to allow full electromagnetics modelling and calculation of the Poynting streamlines.

The challenge of this kind of comparison is that neither the conical monopole, nor the stacked patch is very well matched with the maximum directivity envelope over the full farfield, and so methods like 'mean offset' or correlation functions do not provide an independent metric for the array performance.

If the 'optimum' array is defined as one that matches or exceeds the maximum directivity envelope over the full farfield, this would imply that in all directions the array is as directive as physically possible. One proposed metric that suits this definition is the 'Steering Efficiency Product' (SEP) and the related metric 'Steering Efficiency' (SE) [27]. As defined, this metric was concerned with planar apertures, with the peak aperture efficiency (Equation 5 [28]) at boresight, and continuous beamsteering coverage from boresight to the maximum steering angle for which the beamformed directivity $\geq$ Maximum Directivity-3dB, θ_1.

$$\eta_{ap} = \frac{A_e}{A_p} \tag{5}$$

$$SEP_{1D} = \eta_{ap} \frac{2\theta_1}{2\pi} \tag{6}$$

In one dimension, this was defined as the product of peak aperture efficiency η_{ap} and the fraction of fully circumferential scan (2π radians), Equation 6.

$$SE_{1D} = \frac{\theta_r}{2\pi}, \quad SEP_{1D} = \eta_{ap} \frac{\theta_r}{2\pi} \tag{7}$$

The proposer of this metric was primarily concerned with planar antenna arrays, given the focus on maximum steering

TABLE 1. Beam steering metrics for each element type. maximum directivity, peak aperture efficiency (η_{ap}), steering efficiency (SE), and steering efficiency product (SEP).

	D_{MAX} (dBi)	η_{ap} (%)	SE (%)	SEP (%)
Aperture	14.2	-	38	38
Directional	15	120	40	48
Omnidirectional	12.9	76	33	25
Patch	14.4	106	18	9
Conical	12.7	72	8	6
Conical (Meas)	11.6	55	20	10.6

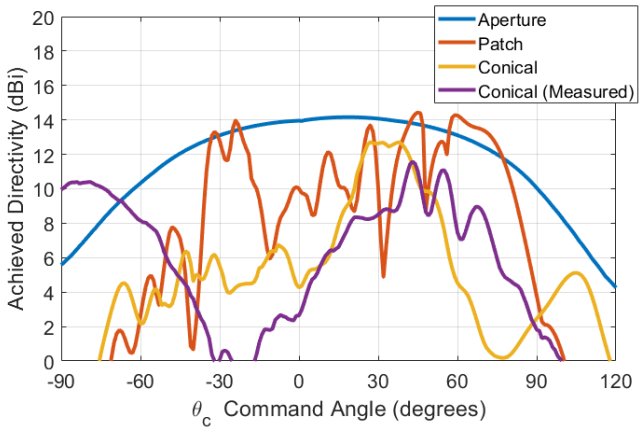

FIGURE 27. Comparison of patch, modelled, & measured monopole main beam achieved directivity with aperture maximum directivity envelope ($\phi = 270°$).

angle. However, the general case could be considered to be an array of arbitrary shape for which the array coverage may not be symmetrical about boresight. Therefore in order to make the metric more robust, instead of maximum steering angle, the integral of the farfield points for which the beamformed directivity $\geq$ Maximum Directivity-3dB, θ_r is used, shown in Equation 7. This can be extended to the two-dimensional steering efficiency product by considering the whole farfield, but since a linear array is considered here it is more appropriate to confine the analysis to the primary steering plane.

The benefit of this metric compared to others, such as maximum directivity or maximum steering angle, is that the steering efficiency product provides a single number encapsulating both of these metrics. This metric also offers a more general understanding of the arrays farfield 'coverage' within 3dB of the maximum directivity, and the efficiency of the aperture in relation to its size. Thus it can be used to distil the farfield performance of an array design to a single number. It does not consider inter-element coupling or array efficiency losses as they are outside the scope of this work.

This metric does, however, highlight the issue with using the physical aperture for array performance metrics. When the aperture efficiency (η_{ap}) in Table 1 is considered it becomes obvious that the stacked patch antenna elements have an 'effective' aperture that is larger than the physical dimensions of the aperture, as previously discussed. In this case, this issue means that the steering efficiency (SE) is a better performance metric to use, as it is not distorted by the uncertainty between the physical and effective apertures. When the steering efficiency is calculated along the prime beamsteering plane ($\phi = 90°, 270°$) there is a clear distinction to be made between the conical monopole elements, and the stacked patches. This can also be seen from the corresponding plot of achieved directivity versus command angle in Figure 27. If the comparable steering efficiency is calculated for the aperture projection, a value of 38% along this plane is observed. In this context the steering efficiency of the arbitrary elements and the stacked patches are very close to the predicted optimum for the aperture itself. As the aperture projection method is based upon the physical aperture of the array, its associated steering efficiency product will also be 18%, and hence this can be used as a metric for an 'optimum' antenna element for the aperture. Any array design that achieves a SEP equal to that of the aperture itself could be considered an 'optimum' array for that aperture. A value of SEP greater than that of the aperture indicates an aperture efficiency of over 100%, in which case the steering efficiency should be considered as a more accurate metric. This also takes into account the maximum directivity of an array. The omnidirectional arbitrary elements also have a steering efficiency consistent with that of the aperture projection results. The conical elements, both modelled and measured, suffer in performance as their radiation null vectors are aligned in the analysis plane, and thus they are being compared in a plane that their inherent pattern produces nulls. Despite this, the measured conical element patterns achieves a steering efficiency of 20% in the plane, and a SEP of 10.5%.

The agreement between the steering efficiency of the aperture itself, the arbitrary elements, and the modelled and measured elements lends confidence to the aperture projection methodology as a whole. While the aperture assessment is a factor in overall magnitudes of the maximum directivity envelope predicted, the agreement in terms of steering efficiency is promising. The directional arbitrary elements are less directive than the stacked patches, and have a greater steering efficiency. The omnidirectional arbitrary elements showed good agreement with the measured conical monopole array performance (1.3dB difference in maximum directivity, 13% difference in steering efficiency), and exhibited good steering efficiency (33%). One promising approach would be the use of 'mixed' directional and omnidirectional elements in order to increase the steering efficiency of the array. In addition, one extension of this approach would be to account for the presence of scatterers like the mounting plate below the array (shown in the background Figure 4) and include its effects on the overall antenna element and beamformed array pattern.

The challenge to both the steering efficiency product metric and to the aperture projection method is the assessment of the 'effective' aperture of an array as discussed in Section III-B. If the assessed aperture is smaller than the actual effective aperture of the array, then the calculated aperture maximum

directivity envelope will be lower in magnitude than the beamformed achieved directivity of the array. This is referred to as aperture boundary uncertainty. While not ideal, as the aperture size increases as a function of wavelength, this effect should be minimized as the boundary uncertainty becomes a smaller proportion of the total aperture.

IV. CONCLUSION

As long as the limitations of the aperture projection model are understood, the maximum directivity envelope predicted by this model provides an excellent way to investigate the performance of a given aperture on an arbitrary platform. The current limitation of this model is that it does not account for array element types, giving a performance envelope for the aperture alone. Combining this method with the steering efficiency and steering efficiency product metrics enables a rapid assessment of the achieved array performance of different antenna array designs for a given aperture. At present this method does not account for the effects of scattering in the surroundings of the antenna elements, such as the spacing of the shield plate in Figure 5, and this inclusion represents a future extension of this method.

There was good agreement between the steering efficiency of the directional arbitrary elements (40%) and that of the stacked patch design (18%), indicating that this arbitrary element is well matched to the performance of the stacked patch element, and a good predictor of the performance and steering efficiency of a directional element in this aperture. If the steering efficiency of the stacked patch elements could be improved, perhaps with a slightly less directional element design, then it would more closely approach the aperture optimum.

The omnidirectional and modelled conical monopole elements were not so well matched. While the maximum directivity, and hence aperture efficiency of both were well matched (75% and 72%), the steering efficiency was highly divergent, with the conical elements exhibiting a reduction in steering efficiency of 25%. This is likely due to the conical monopoles wider element pattern nulls, and farfield ripple, suppressing the achieved directivity of the conical monopole array throughout the steering plane. When the measured conical monopole elements are considered, there is much greater agreement in terms of steering efficiency (20%), while the aperture efficiency is reduced (55%).

The aperture projection model provides a useful predictor of the potential beamformed directivity of an antenna array on a given platform. While neither this method, nor the arbitrary antenna elements considered include the effects of scattering on the overall antenna patterns, the aperture projection method offers a worthwhile understanding of the beamformed directivity envelope of the aperture. This is acceptable for a starting point, allowing rapid assessment of the suitability of an aperture on platform with a very limited information set (frequency, aperture & platform geometry). Further development would focus on the inclusion of environmental scatterers on the antenna patterns, and improved methods for representing idealised antenna types.

ACKNOWLEDGMENT

Data are available at the University of Bristol data repository, data.bris, at https://doi.org/10.5523/bris.26ouj8j75ss112mc96y3hi0bnd.

REFERENCES

[1] L. Josefsson and P. Persson, *Conformal Array Antenna Theory and Design*. Hoboken, NJ, USA: Wiley, 2006, doi: 10.1002/047178012x.

[2] A. Ahmadi, A. Kosari, and S. M. B. Malaek, "A generic method for remote sensing satellites conceptual design and rapid sizing based on 'design for performance' strategy," *IEEE Aerosp. Electron. Syst. Mag.*, vol. 33, no. 2, pp. 34–51, Feb. 2018, doi: 10.1109/MAES.2018.170052.

[3] J. Kmetzo, "An analytical approach to the coverage of a hemisphere by N planar phased arrays," *IEEE Trans. Antennas Propag.*, vol. AP-15, no. 3, pp. 367–371, May 1967, doi: 10.1109/TAP.1967.1138933.

[4] M. Skolnik, *Introduction to Radar Systems*. New York, NY, USA: McGraw-Hill, 1982, p. 64.

[5] A. Jablon and A. Agrawal, "Optimal number of array faces for active phased array radars," *IEEE Trans. Aerosp. Electron. Syst.*, vol. 42, no. 1, pp. 351–360, Jan. 2006, doi: 10.1109/TAES.2006.1603428.

[6] Computer Simulation Technologies. *Microwave Studio*. [Online]. Available: https://www.cst.com

[7] Z. Cendes, "The development of HFSS," in *Proc. USNC-URSI Radio Sci. Meeting*, Jun. 2016, pp. 39–40, doi: 10.1109/USNC-URSI.2016.7588501.

[8] T. E. Morton and K. M. Pasala, "Performance analysis of conformal conical arrays for airborne vehicles," *IEEE Trans. Aerosp. Electron. Syst.*, vol. 42, no. 3, pp. 876–890, Jul. 2006, doi: 10.1109/TAES.2006.248218.

[9] C. Balanis and C. Cockrell, "Analysis and design of antennas for air traffic collision avoidance systems," *IEEE Trans. Aerosp. Electron. Syst.*, vol. AES-7, no. 5, pp. 960–967, Sep. 1971, doi: 10.1109/TAES.1971.310337.

[10] P. H. Pathak, P. Janpugdee, and R. J. Burkholder, "A comparison of two different ray based methods for analyzing large convex conformal antenna arrays," in *Proc. 4th Eur. Conf. Antennas Propag.*, Apr. 2010, pp. 1–5.

[11] T. Pelham, G. Hilton, E. Mellios, and R. Lewis, "Predicting conformal aperture gain from 3-D aperture and platform models," *IEEE Antennas Wireless Propag. Lett.*, vol. 16, pp. 700–703, 2017, doi: 10.1109/LAWP.2016.2600403.

[12] *IEEE Standard Definitions of Terms for Antennas*, Mar. 2014, pp. 1–50, doi: 10.1109/IEEESTD.2014.6758443.

[13] P. Hannan, "The element-gain paradox for a phased-array antenna," *IEEE Trans. Antennas Propag.*, vol. AP-12, no. 4, pp. 423–433, Jul. 1964, doi: 10.1109/TAP.1964.1138237.

[14] *Boeing ScanEagle*. [Online]. Available: https://www.naval-technology.com/projects/scaneagle-uav/

[15] *Northrop Grumman X-47B*. [Online]. Available: https://www.naval-technology.com/projects/x-47b-unmanned-combat-air-system-carrier-ucas/

[16] *JSTARS E-8C*. [Online]. Available: https://www.airforce-technology.com/projects/jstars/

[17] T. Buttler, *The De Havilland Sea Vixen*. Tonbridge, U.K.: Air-Britain, 2007.

[18] T. Pelham, R. Lewis, E. Mellios, and G. Hilton, "Predicting conformal aperture directivity for arbitrary curved surfaces," in *Wideband and Multi-Band Antennas and Arrays for Civil, Security [amp] Military Applications*. London, U.K.: Institution Engineering Technology, 2015, pp. 1–3, doi: 10.1049/ic.2015.0147.

[19] D. Brennan, "Linear diversity combining techniques," *Proc. IRE*, vol. 47, no. 6, pp. 1075–1102, Jun. 1959, doi: 10.1109/JRPROC.1959.287136.

[20] N. J. Bershad, "On the real and complex least mean square adaptive filter algorithms," *Proc. IEEE*, vol. 69, no. 4, pp. 469–470, Apr. 1981, doi: 10.1109/proc.1981.11993.

[21] R. Nagal, P. Kumar, and P. Bansal, "Performance analysis of least mean square algorithm for different step size parameters with different filter order and iterations," in *Proc. Int. Conf. Recent Develop. Control, Autom. Power Eng. (RDCAPE)*, Mar. 2015, pp. 326–331, doi: 10.1109/RDCAPE.2015.7281418.

[22] E. Nicolau, *Adaptive Arrays/by Edmond Nicolau Dragoi Zaharia* (Studies in Electrical and Electronic Engineering), vol. 35. Amsterdam, The Netherlands: Elsevier, 1989.
[23] P. Elliot, "Conformal array beam synthesis and taper efficiency comparisons," MITRE, Tech. Rep., 2005. [Online]. Available: https://www.mitre.org/publications/technical-papers/conformal-array-beam-synthesis-and-taper-efficiency-comparisons
[24] H. Zhai, S. Tjuatja, J. W. Bredow, and M. Lu, "A quasi-planar conical antenna with broad bandwidth and omnidirectional pattern for ultrawideband radar sensor network applications," *IEEE Trans. Antennas Propag.*, vol. 58, no. 11, pp. 3480–3489, Nov. 2010, doi: 10.1109/TAP.2010.2072899.
[25] C. J. Railton, D. L. Paul, and I. J. Craddock, "Analysis of a 17 element conformal array of stacked circular patch elements using an enhanced FDTD approach," *IEE Proc.-Microw., Antennas Propag.*, vol. 150, no. 3, pp. 153–158, Jun. 2003, doi: 10.1049/ip-map:20030417.
[26] J. Diao and K. F. Warnick, "Practical superdirectivity with resonant screened apertures motivated by a Poynting streamlines analysis," *IEEE Trans. Antennas Propag.*, vol. 66, no. 1, pp. 432–437, Jan. 2018, doi: 10.1109/TAP.2017.2772929.
[27] J. G. Marin and J. Hesselbarth, "Figure of merit for beam-steering antennas," in *Proc. 12th German Microw. Conf. (GeMiC)*, Mar. 2019, pp. 44–47, doi: 10.23919/GEMIC.2019.8698122.
[28] J. Kraus and R. J. Marhefka, *Antennas for All Applications*, 3rd ed. New York, NY, USA: McGraw-Hill, 2003.

TIMOTHY G. PELHAM (Member, IEEE) received the M.Phys. degree (Hons.) in physics from the University of Surrey, in 2009, and the Ph.D. degree from the University of Bristol, in 2018, with research into conformal antenna array design. He worked with the Oak Ridge National Laboratory, TN, USA. In 2011, he joined MBDA, as a Systems Engineer, before becoming a Senior Systems Engineer. He is currently working as a Senior Research Associate in mmWave wireless with the University of Bristol.

GEOFF HILTON received the B.Sc. degree (Hons.) in electrical and electronic engineering from the University of Leeds, in 1984, and the Ph.D. degree from the University of Bristol, in 1993, with a research into printed antenna elements. Subsequently, he joined Marconi Command and Control Systems as a Design and Development Engineer. In 1989, he became a Research Assistant with the University of Bristol, working on antenna array design for a radar application. In 1993, he was appointed as a Lecturer with the department and promoted to a Senior Lecturer, in 2004.

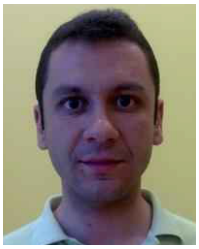

EVANGELOS MELLIOS received the Diploma degree in electrical and computer engineering from the Aristotle University of Thessaloniki, in 2007, the M.Sc. degree in communication systems and signal processing from the University of Bristol, in 2008, and the Ph.D. degree from the Communication Systems and Networks Research Group, in 2013. He is currently a Lecturer in electrical and electronic engineering with the University of Bristol.

ROB LEWIS (Member, IEEE) was a Group Leader with the BAE System's Advanced Technology Centre, Department of Sensor Systems, Chelmsford, U.K. The Group focuses on all aspects of electromagnetic engineering including antenna design, installed antenna performance prediction, radar cross-section control, and technical consultancy. Applications include air, sea, land, and space systems in both military and civil domains. He has over 25 years experience in microwave and antenna design and has published numerous papers and patents. His research interests include antennas for wideband and multifunction sensor systems. He has served as a Deputy Chairman for a NATO investigation of naval antenna systems, and on the organising and technical committees for the EuCAP Conference series, the IET Technical committees, the LAPC Technical Committee.